Parallel double-plate capacitive proximity sensor modelling based on effective theory

Nan Li, Haiye Zhu, Wenyu Wang, and Yu Gong

Citation: AIP Advances **4**, 027119 (2014); doi: 10.1063/1.4866986
View online: http://dx.doi.org/10.1063/1.4866986
View Table of Contents: http://scitation.aip.org/content/aip/journal/adva/4/2?ver=pdfcov
Published by the AIP Publishing

AIP ADVANCES **4**, 027119 (2014)

Parallel double-plate capacitive proximity sensor modelling based on effective theory

Nan Li,[a,b] Haiye Zhu, Wenyu Wang, and Yu Gong
Research Center for Non-destructive Testing and Evaluation, Beijing University of Technology, Beijing100124, China

(Received 4 August 2013; accepted 14 February 2014; published online 25 February 2014)

A semi-analytical model for a double-plate capacitive proximity sensor is presented according to the effective theory. Three physical models are established to derive the final equation of the sensor. Measured data are used to determine the coefficients. The final equation is verified by using measured data. The average relative error of the calculated and the measured sensor capacitance is less than 7.5%. The equation can be used to provide guidance to engineering design of the proximity sensors. [http://dx.doi.org/10.1063/1.4866986]

I. THE MANUSCRIPT

Capacitive proximity sensor technique has been developed for decades. There are two main types of capacitive proximity sensors based on different structure: parallel-plate and coplanar-plate based on fringe effect theory (the proximity sensor). In 1969, Notltingk[1] proposed two sensor structures based on fringe effect: rectangular and ring-shape. The measurement results were reported for different arrangements, such as different gaps between sensor electrodes, different screen thickness, and different screen protrusion. However, the analytical formula is not considered at that moment, the optimization process is only based on experimental results. Later, Notlingk *et al.*[2] introduced a novel proximity structure, with two live electrodes, separated by an earthed screen. The variation of characteristics with geometrical details has been established experimentally, allowing optimum designs to be made to meet any chosen performance specification. However, there is no analytical equations are provided. In 1993, Luo and Chen[3] presented an innovative proximity sensor using the micro-electro-mechanical system (MEMS) technology, and derived a mathematical model for a ring-shape capacitive proximity sensor. However, the equation for the fringing capacitance is very complicated and it has an infinite summation involving the modified Bessel functions which themselves have infinite summations. A. V. Mamishev *et al.*[4–6] did a series of research on interdigital sensor structure, including sensor multi-wavelength optimization, sensor modeling and sensor structure improvement, and all of these work are based on experimental results and simulation results. Meanwhile, the capacitive proximity sensor technique has been applied to some areas, such as civil engineering, agriculture and manufacture industries. Sundara-Rajan *et al.*[7] presented the use of fringing field interdigital sensors to measure moisture concentration in paper pulp at moisture levels as high as 96%. Yang Liu *et al.*[8] have developed a coplanar electrode capacitance sensor to detect the moisture content in the crop and the measuring error is only 1%. In civil engineering field, T. Bore *et al.*[9] have used the capacitive probe based on fringe effect principle to detect the both voids and white paste in ducts of bridges without having to open them and achieve good performance. Amr A Nassr *et al.*[10] have designed a capacitive proximity sensor to detect the water intrusion in composite structures by evaluating the dielectric properties of different composite system constituent materials,

[a]This research was performed while Nan Li was at Research Center for Non-destructive Testing and Evaluation, Beijing, 100124.
[b]Electronic mail: nan.li@bjut.edu.cn

and in his another paper,[11] a capacitive proximity sensors to detect air voids, water intrusion, and glue infiltration damages in fiber-reinforced polymers-strengthened concrete structures has been introduced. For simplest proximity sensor structure, Morgan[12] has presented an analytical model of the basic SAW (Surface acoustic wave) transducers, and later, Engan,[13] Datta and Hunsinger[14] have calculated the admittance of the basic SAW (Surface acoustic wave) transducers, and these models are available for capacitive proximity sensor structures, However, these mathematical models and analytical equations is also too complicate to be applied for sensor design directly. In 2004, Chen *et al.*[15] made an analytical model for coplanar capacitive sensing of droplets for microfluidic devices. The paper focuses on an interdigitated sensor structure. The analytical model for coplanar capacitive sensing is two-dimension without considering the length of the electrode. A modelling of concentric coplanar capacitive sensor is presented for the quantitative characterization of material properties for multi-layered dielectrics by Chen *et al.*[16,17] Electrostatic Green's functions are derived by utilizing the Hankel transform given the cylindrical symmetry of the proposed sensor. The sensor surface charge distribution is calculated using the method of moments. In 2013, Cheng *et al.*[18] discussed a concentric coplanar capacitor in 'epidermal' format yield analytic expressions of the impedance for single- and double-layer capacitors also by using Hankel transform. The capacitance is also calculated by finite element method (FEM) to validate the analytical model by using the thermal module in the FEM program ABAQUS. Due to the curvature of electric flux in coplanar structure, the equation of capacitance for this structure is normally approximated by conformal mapping technique using an inverse cosine transform, and the analytical equations derived has a complex structure. Therefore, in this paper, we aims to derive a semi-analytical model based on the effective theory which can provide guidance to engineering design of the double-plate coplanar capacitive sensors with a simple formula expression.

In principle, capacitance calculation is an application of ordinary electrodynamics. However, with specific boundary conditions and the impedance analyzer measurements, the equations for calculation of capacitance are non-linear, which makes it difficult to obtain a theoretical model respond to real measurement. Fortunately, the effective theory, which is widely used in theoretical physics and condensed matter physics, can be used to deal with the non-linear equations. The key point of the effective theory is that the basic theory presents differently in different scale. Thus, the theoretical estimation formulas can be used to match the corresponding coefficients, as an effective theory. Also, the renormalization group evolution can be used to estimate the application sphere of the theory. In this paper, we will use this method for estimation of the capacitance of sensors.

The paper is organized as follows. The effective theory for analyzing proximity capacitive sensors is presented and primary formulation is derived in the second part. The physical models for the sensors are proposed. Then the experimental results are given to indicate that the expression to describe the relationship between those sensor design parameters is effective and feasible.

II. EFFECTIVE THEORY AND PHYSICAL MODELS FOR SENSORS

An effective theory is proposed to describe a certain set of observations, i.e. the basic theory of a system is always highly non-linear. The basic theory can be used to estimate a real system, leaving some coefficients to be determined by experiment, which is called matching. With a non-linear theory, renormalization group running can be used to estimate the form the effective formula.

Considering a simplest proximity sensor structure, which consists of two plates: E1 and E2, as shown in Fig. 1, one plate is applied an AC excitation, and the other for detection.

The electrodes have same size, and the thickness of the electrodes is negligible. The boundary conditions can be described as

$$\begin{cases} \nabla^2\varphi = 0, & \text{in } \Omega \\ \varphi\,|_{\Gamma_1} = \varphi_0, & \text{on source electrode} \\ \varphi\,|_{\Gamma_2} = 0, & \text{on detective eletrode} \end{cases} \tag{1}$$

where, Γ_1 and Γ_2 refer to the surface of the source and detection electrodes, respectively. Ω is volume above the sensor electrodes. In general, if a formula is used to calculate the capacitance of

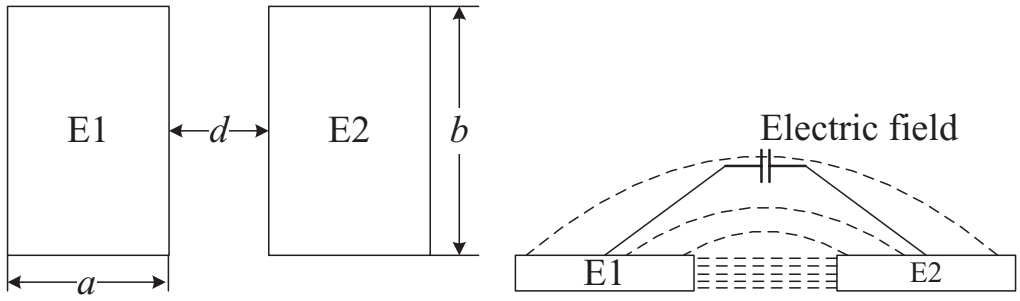

FIG. 1. Simplest capacitive proximity sensor structure (top view on the left, and side view on the right).

the proximity sensor analytically, the capacitance, C, is a function of the parameter a, b, and d, where a and b are the width and length of the electrode, and d refers to the space between the electrodes. C can be divided in two parts:

$$C = f(a, b, d) = q(\tau, b, d)g(t_1, t_2) \tag{2}$$

where $q(\tau, b, d)$ is scale-dependent, τ is a typical length of the sensor, and a, b or d can be chosen as the scale parameters. This function means that if all the parameters are enlarged 100 times, $q(\tau, b, d)$ must be changed greatly according to the scale parameter τ. For example, if $\tau = a$, then $t_1 = 1 + \frac{b}{a}$, $t_2 = \frac{d}{a}$. Because $g(t_1, t_2)$ is scale-independent, if the scale of the sensor is enlarged, this function will not change as it depends on t_1 and t_2. Note that if the basic theory of a system is linear, $g(t_1, t_2)$ will be a constant. In the analysis of sensor capacitance, the basic theory of the system is non-linear. Therefore, similar renormalization group running can be used to estimate $g(t_1, t_2)$. Thus,

$$\frac{C}{q(\tau, b, d)} = g(t_1, t_2) \tag{3}$$

Because $g(t_1, t_2)$ is scale-independent,

$$\frac{dg(t_1, t_2)}{d\tau} = \frac{\partial g(t_1, t_2)}{\partial t_1} \cdot \frac{dt_1}{d\tau} + \frac{\partial g(t_1, t_2)}{\partial t_2} \cdot \frac{dt_2}{d\tau} = 0$$

Note that because a is chosen as the scale parameter, and $t_1 = 1 + \frac{b}{a}, t_2 = \frac{d}{a}$, the scale parameter will be in the denominator of t_1, t_2. Thus,

$$\begin{aligned} &\frac{\partial g(t_1, t_2)}{\partial t_1} \cdot t_1 + \frac{\partial g(t_1, t_2)}{\partial t_2} \cdot t_2 = 0 \\ &\Rightarrow \frac{\partial g(t_1, t_2)}{\partial \ln t_1} + \frac{\partial g(t_1, t_2)}{\partial \ln t_2} = 0 \end{aligned} \tag{4}$$

The formula is the similar β function as in the quantum field theory.[19] Then, the variable separation method can be used to estimate $g(t_1, t_2)$ and can be expressed as

$$g(t_1, t_2) = M(\ln t_1) \cdot N(\ln t_2) \tag{5}$$

Where, $\ln t_1$ and $\ln t_2$ are variables. From Eq. (4) and Eq. (5),

$$\begin{aligned} &\frac{\partial g(t_1, t_2)}{\partial \ln t_1} + \frac{\partial g(t_1, t_2)}{\partial \ln t_2} \\ &= N(\ln t_2) \cdot \frac{\partial M(\ln t_1)}{\partial \ln t_1} + M(\ln t_1) \cdot \frac{\partial N(\ln t_2)}{\partial \ln t_2} = 0 \end{aligned}$$

$$\Rightarrow \frac{\partial \ln M(\ln t_1)}{\partial \ln t_1} = -\lambda_i,$$
$$\frac{\partial \ln N(\ln t_2)}{\partial \ln t_2} = \lambda_i$$

Both equations are independent of each other. Thus λ_i must be a constant.

$$\Rightarrow M(\ln t_1) = {t_1}^{-\lambda_i}, N(\ln t_2) = {t_2}^{\lambda_i}$$

Therefore, $g(t_1, t_2)$ can be obtained as

$$g(t_1, t_2) = \sum \alpha_i g_i(t_1, t_2) = \sum_{i=1}^{n} \alpha_i {t_1}^{-\lambda_i} \cdot {t_2}^{\lambda_i}, (n = 1, 2, 3 \cdots) \tag{6}$$

Finally, the capacitance of the proximity sensor is

$$C = q(\tau, b, d) \sum_{i=1}^{n} \alpha_i {t_1}^{-\lambda_i} \cdot {t_2}^{\lambda_i} \tag{7}$$

If a good estimation is chosen, then the first term of $g(t_1, t_2)$ is principal(fundamental) order. Also, it can be expanded order by order to give more precise estimation. The capacitance can be written as:

$$\begin{aligned} C &= q(\tau, b, d) \sum_{i=1}^{n} \alpha_i {t_1}^{-\lambda_i} \cdot {t_2}^{\lambda_i} \\ &= \alpha_1 \cdot q(\tau, b, d) \cdot {t_1}^{-\lambda_1} \cdot {t_2}^{\lambda_1} \cdot \left(1 + \frac{\alpha_2}{\alpha_1} {t_1}^{-\lambda_2} \cdot {t_2}^{\lambda_2} + \cdots + \frac{\alpha_n}{\alpha_1} {t_1}^{-\lambda_2} \cdot {t_2}^{\lambda_2}\right) \\ &= \alpha_1 \cdot q(\tau, b, d) \cdot {t_1}^{-\lambda_1} \cdot {t_2}^{\lambda_1} \cdot \circ(t_1, t_2) \\ (n &= 1, 2, 3 \cdots) \end{aligned}$$

where, α_i is the accommodation coefficient. $\circ(t_1, t_2)$ is a higher order part. After estimation of $g(t_1, t_2)$ the basic theory can be used to obtain the estimation of $q(\tau, b, d)$. Therefore, three physical models are established according to the effective theory.

A. Physical model 1

Assumption 1: Let's assume that the sensor plate is infinitely large. The final analytical formulation is related to the original formulation of parallel-plate capacitor. The capacitance C can be derived from Eq. (8):

$$C = \varepsilon \cdot b \frac{a}{d} \tag{8}$$

where, ε is the relative permittivity. Thus, electric charge distribution mainly depends on length b.

B. Physical model 2

Assumption 2: Let's assume $b \to \infty$, and $d \to 0$. Two parallel plates are simplified as two parallel lines, since C mainly depends on the area of the electrodes. Thus, Eq. (8) can be changed to Eq. (9):

$$C = \eta \cdot \varepsilon \cdot b \cdot \left(\frac{a}{d}\right)^{\chi} \tag{9}$$

where, η is a constant, and χ is a correction factor.

TABLE I. Design parameters of capacitive proximity sensor.

No.	Aspects			
	Length of electrode (b) (mm)	Width of electrode (a) (mm)	Aspect ratio (b/a)	Area of electrodes (mm^2)
N1	25.0	25.0	1:1	$625 + 0.00$
N2	56.0	11.2	5:1	$625 + 2.20$
N3	79.0	7.9	10:1	$625 - 0.90$
N4	97.5	6.5	15:1	$625 + 8.75$

TABLE II. Measured capacitance and calculated values of the sensor based on Table I setups.

No.	Distance									
	*d*1 (2 mm)		*d*2 (4 mm)		*d*3 (6 mm)		*d*4 (8 mm)		*d*5 (10 mm)	
	Mea. (pF)	*Calc.* (pF)	*Mea.* (pF)	*Calc.* (pF)	*Mea.* (pF)	*Calc.* (pF)	*Mea.* (pF)	*Calc.* (pF)	*Mea.* (pF)	*Calc.* (pF)
N1	0.2688	0.2290	0.1914	0.1993	0.1516	0.1566	0.1197	0.1306	0.1073	0.1123
N2	0.5378	0.5172	0.3524	0.3283	0.2359	0.2495	0.2014	0.2035	0.1580	0.1723
N3	0.6119	0.6957	0.5011	0.4382	0.3594	0.3315	0.3074	0.2698	0.2435	0.2284
N4	0.8409	0.8485	0.5130	0.5331	0.3905	0.4029	0.3161	0.3280	0.2509	0.2779

C. Physical model 3

Let's consider the practical conditions, when b is fixed, and $d \to \infty$, $C \to 0$. Similarly, when $d \to 0$,$C \to C_{\max}$, the capacitance mainly depends on d. Thus, χ satisfies Eq. (10):

$$\chi = \begin{cases} 1 & b \ll d, b > 0, d > 0 \\ \frac{2}{\pi} \arctan\left(\frac{d}{b}\right), & others, b > 0, d > 0 \\ 0 & b \gg d, b > 0, d > 0 \end{cases} \tag{10}$$

Therefore, C can be expressed as

$$C = \eta \cdot \varepsilon \cdot b \cdot \left(\frac{a}{d}\right)^{\frac{2}{\pi}\arctan\left(\frac{d}{b}\right)} \cdot X^{\beta} \cdot Y^{\gamma} \tag{11}$$

where, X and Y are scale-independent, and η, β and γ can be calculated according to the series of experimental results.

III. EXPERIMENTS

Experiment conditions are as follows: The excitation frequency is 500 kHz. The AC supply is 0.5V. The electrodes are made of flexible copper, and earthed shielding plate is arranged under the sensor, the capacitances of the sensor are measured by Impedance Analyzer Agilen 4294A. The areas of the sensors are almost the same but with different aspect ratio. The detailed information is listed in Table I.

Measured capacitance and calculated values are listed in Table II. According to the experimental results, η, β and γ are determined respectively, and the final formulation can be expressed as

$$\begin{aligned} C &= \frac{7}{40} \cdot \varepsilon \cdot b \cdot \left(\frac{a}{d}\right)^{\frac{2}{\pi}\arctan\left(\frac{d}{b}\right)} \cdot \left(1 + \frac{b}{a}\right)^{\frac{1}{3}} \cdot \left(\frac{d}{a}\right)^{-\frac{2}{3}} \\ &= \frac{7}{40} \cdot \varepsilon \cdot b \cdot \left(\frac{a}{d}\right)^{\frac{1}{3}+\frac{2}{\pi}\arctan\left(\frac{d}{b}\right)} \cdot \left(1 + \frac{b}{a}\right)^{\frac{1}{3}} \cdot \left(\frac{d}{a}\right)^{-\frac{1}{3}} \end{aligned} \tag{12}$$

The theoretical results and experimental results are compared in Fig. 2.

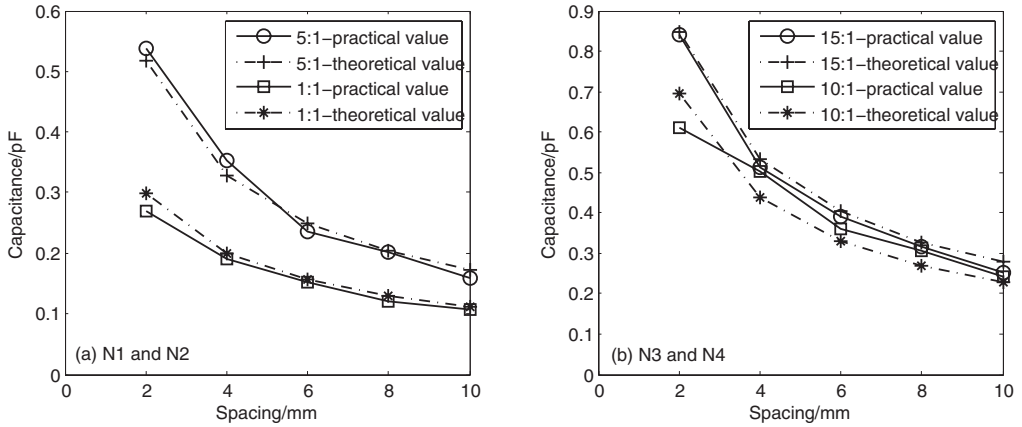

FIG. 2. Comparisons of calculated and experimental values.

TABLE III. Relative errors between measurements and calculated values.

No.	Distance					Ave. error
	$d1$ (2 mm)	$d2$ (4 mm)	$d3$ (6 mm)	$d4$ (8 mm)	$d5$ (10 mm)	
N1	11.22%	4.17%	3.27%	9.11%	4.64%	6.48%
N2	3.82%	6.83%	5.73%	1.01%	9.03%	5.29%
N3	13.70%	12.56%	7.76%	12.21%	6.22%	10.49%
N4	0.91%	3.90%	3.20%	3.76%	10.75%	4.50%

The accuracy of the theoretical value is evaluated by

$$e = \frac{C - \overline{C_m}}{\overline{C_m}} \times 100\% \tag{13}$$

where, $\overline{C_m}$ is the mean measured value, C is the calculated value by Eq. (12). The relative errors between measurements and calculated values are listed in Table III.

Fig. 2 shows the comparison of the calculated and experimental values, indicating the effectiveness of Eq. (12). The total average relative error is 6.69%. Considering the proximity sensor capacitance changes is non-linear, and it depends on spacing d, especially when d is small, when the aspect ratios of the sensor electrodes are 1:1, 5:1 and 15:1, the calculated and measured values are more consistent. However, an obvious error appears in an aspect ratio of 10:1. Note that the curve trend of measured values with aspect ratio of 10:1 shown in Fig. 2(b) is almost linear. Therefore, the difference between the calculated and measured values is introduced by the measurement error.

To further verify the validity of Eq. (12), more experiments are processed with follows setups:

(a) More distance changes between the electrodes are considered with the same aspect ratio as listed in Table I. Measured and calculated capacitance. The total average relative error is 6.05% which can be derived from Table IV, and the experimental results are shown in Fig. 3.

Fig. 3 shows the comparison of the calculated and measurement values with aspect ratios of 1:1, 5:1, 10:1 and 15:1, respectively. The total average relative errors between the measurements and calculated values is 6.05%.

(b) Different aspect ratio of sensor electrode with the distance between electrodes increasing from 1 mm to 10 mm at interval of 1 mm. The experimental conditions are setup as shown in Table V.

The results are listed in Table VI. The theoretical results and experimental results are compared in Fig. 4.

Fig. 4 shows the comparison of the calculated and measurement values with aspect ratios of 3:1, 7:1, 9:1 and 20:1, respectively. The curves trend of the measured values with four

TABLE IV. Measured capacitance and calculated values of the sensor based on Table I setups.

	Distance										
	*d*1 (1 mm)		*d*2 (3 mm)		*d*3 (5 mm)		*d*4 (7 mm)		*d*5 (9 mm)		
No.	*Mea.* (pF)	*Calc.* (pF)	*Mea.* (pF)	*Calc.* (pF)	*Mea.* (pF)	*Calc.* (pF)	*Mea.* (pF)	*Calc.* (pF)	*Mea.* (pF)	*Calc.* (pF)	Ave. error
N1	0.4603	0.4531	0.2578	0.2358	0.1879	0.1748	0.1460	0.1423	0.1239	0.1208	4.43%
N2	0.8321	0.8115	0.4054	0.3970	0.3026	0.2827	0.2384	0.2239	0.1927	0.1866	8.50%
N3	1.1030	1.0984	0.5813	0.5316	0.3944	0.3763	0.3157	0.2972	0.2486	0.2473	3.99%
N4	1.3221	1.3426	0.6266	0.6474	0.4262	0.4575	0.3561	0.3612	0.2448	0.3008	7.30%

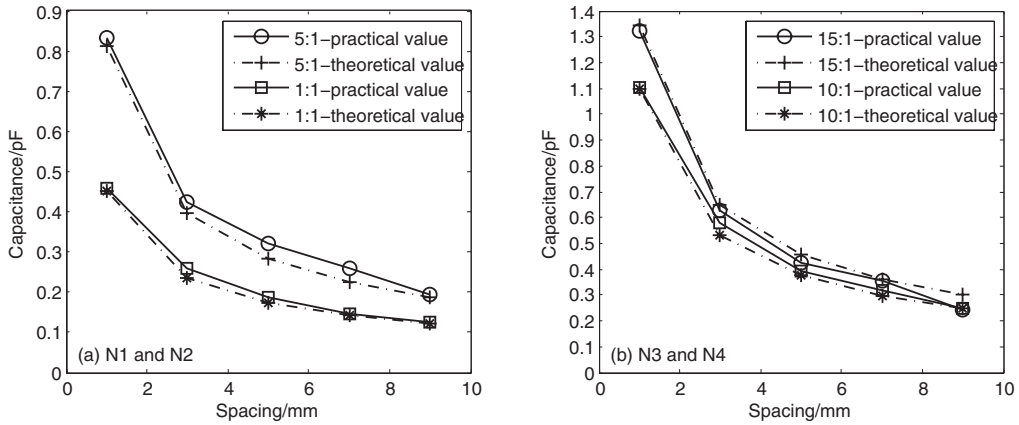

FIG. 3. Comparisons of calculated and experimental values with distance from 1 mm to 9 mm at intervals of 2 mm.

TABLE V. Design parameters of capacitive proximity sensor.

	Aspects			
No.	Length of electrode (b) (mm)	Width of electrode (a) (mm)	Aspect ratio (b/a)	Area of electrodes (mm^2)
N5	43.2	14.4	3:1	$625 - 2.92$
N6	66.5	9.5	7:1	$625 + 6.75$
N7	74.7	8.3	9:1	$625 - 4.99$
N8	112.0	5.6	20:1	$625 + 2.20$

aspect ratios is similar. The average error with aspect ratios of 3:1 and 20:1 are around 10%. The possible reasons are a) because the error calculated by Eq. (13) and the average measured values are very small, small numerical deviation will lead to large relative error, and b) the measurement error occurred during impedance analyzer operation. The total average relative errors between the measurements and calculated values is 7.21%

(c) The capacitance is also calculated by finite element method (FEM) program in COMSOL to validate the analytical model. The simulation conditions are set as same as Table I. The theoretical results and results calculated by COMSOL are compared in Fig. 5, and the comparison of the normalized capacitance is shown in Fig. 6

Because the actual experimental conditions cannot be completely consistent with the numerical simulation, such as frequency of the excitation (Frequency does affect the measurement results actually), ambient noise, etc, the actual measurement results are smaller than the numerical results, and the difference is 0.5–0.8pF between the calculation values based on actual experiments and the numerical simulation values based on FEM program in COMSOL.

TABLE VI. Measured capacitance and calculated values of the sensor based on Table V setups.

	Distance										
	*d*1 (2 mm)		*d*2 (4 mm)		*d*3 (6 mm)		*d*4 (8 mm)		*d*5 (10 mm)		
No.	*Mea.* (pF)	*Calc.* (pF)	*Mea.* (pF)	*Calc.* (pF)	*Mea.* (pF)	*Calc.* (pF)	*Mea.* (pF)	*Calc.* (pF)	*Mea.* (pF)	*Calc.* (pF)	Ave. error
N5	0.4429	0.4201	0.3056	0.2692	0.2423	0.2058	0.1919	0.1684	0.1675	0.1429	11.81%
N6	0.5940	0.6002	0.3849	0.3793	0.2956	0.2875	0.2312	0.2342	0.1996	0.1983	1.44%
N7	0.7212	0.6600	0.4555	0.4160	0.3268	0.3149	0.2551	0.2563	0.1988	0.2169	6.06%
N8	1.1326	0.9627	0.7246	0.6040	0.5101	0.4563	0.3880	0.3715	0.3187	0.3149	9.52%

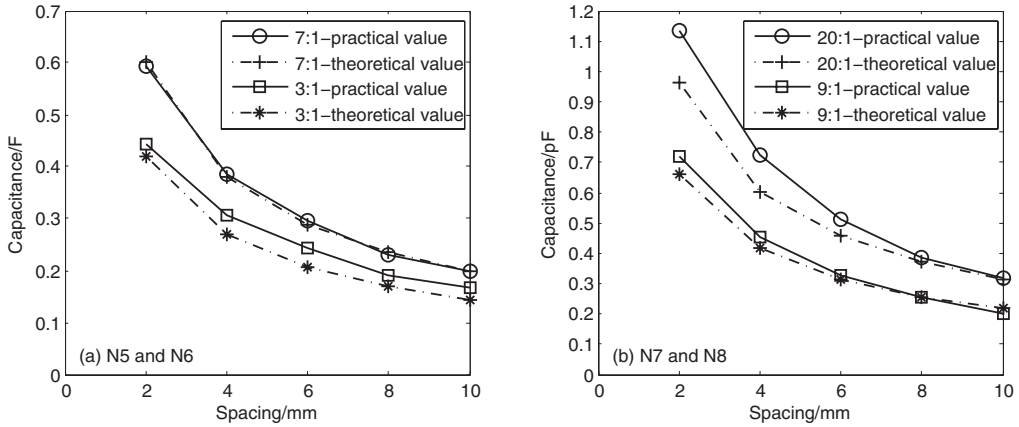

FIG. 4. Further validation of Eq. (5), by comparison of calculated and experimental values.

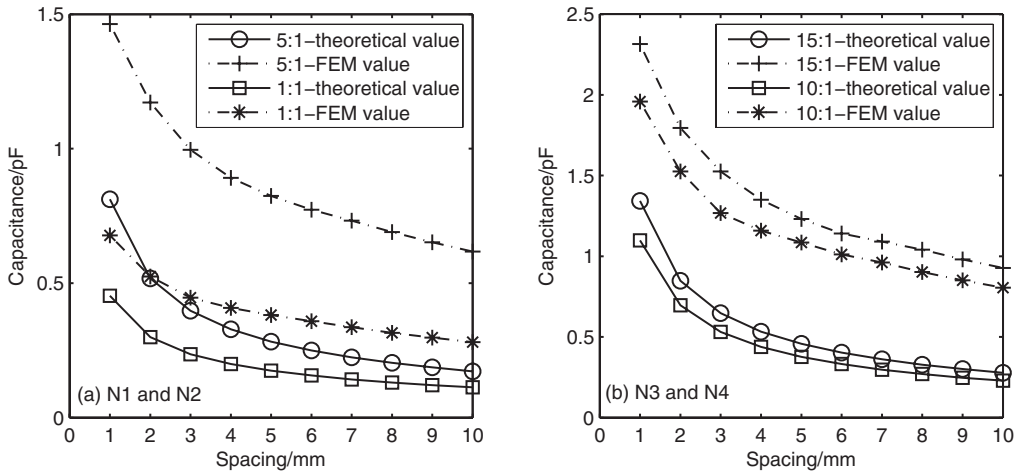

FIG. 5. Further validation of Eq. (5), by comparison of calculated and numerical simulation values.

This does not affect the validity of the semi-analytical formula, according to Fig. 6, the normalized results have a good fit which prove that the formula in the paper still can be applied to guide the actual sensor engineering design.

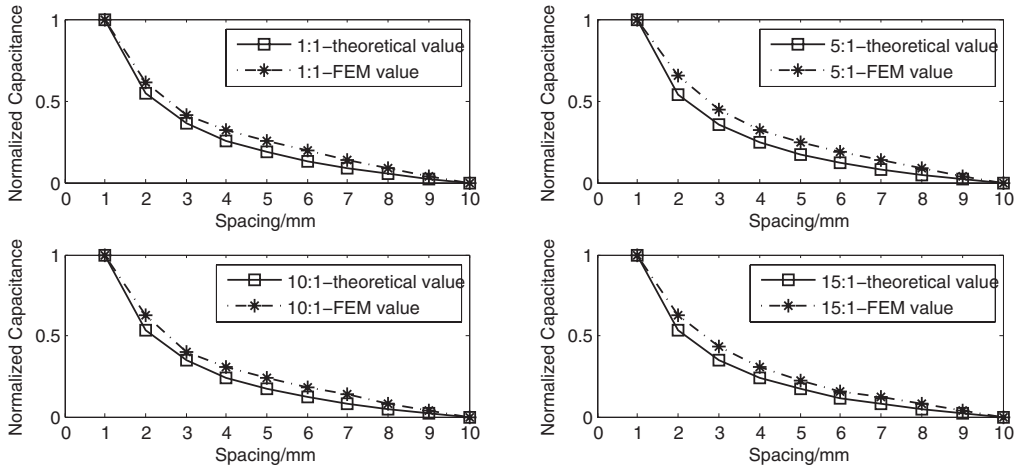

FIG. 6. Comparison of normalized results based on calculated and numerical simulation values.

IV. CONCLUSIONS

The main conclusions are as follows. A semi-analytical model for a double-plate capacitive proximity sensor is presented according to the effective theory. Comparison of the calculated and the measured sensor capacitance with different design parameters indicates that the expression derived by the three established physical models are valid. The average relative error of the calculated and the measured sensor capacitance is less than 7.5%. The equation can be used to provide guidance to engineering design of the proximity sensors.

ACKNOWLEDGMENTS

This work was partially supported by a project funded by National Natural Science Foundation of China (51105008), by Scientific Research Common Program of Beijing Municipal Commission of Education (KM201310005034), and supported by the Zhejiang Open Foundation of the Most Important Subjects. Dr. Li would like to thank the Prof. Wuqiang Yang and Dr. Wuliang Yin for their invaluable help.

[1] B. E. Noltingk, A. E. T. Nye, and H. J. Turner, in *Proc. ACTAIMEKO* (1976) pp. 537–549.
[2] B. E. Noltingk, J. Sci. Instru. **2**, 356–360 (1969).
[3] R. C. Luo and Z. H. Chen, *IEEE/RSJ international Conference on Intelligent Robots and Systems* (Yokohama, Japan, 1993) pp. 1709–1716.
[4] A. V. Mamishev, B. C. Leieutre, and M. Zahn, IEEE Trans. Dielectr. Electr. Insul. **5**(3), 408–420 (1998).
[5] A. V. Mamishev, Y. Du, J. H. Bau, and B. C., IEEE Trans. Dielectr. Electr. Insul. **8**(5), 785–798 (2001).
[6] X. B. Li, G. Rowe, V. Inclan, and A. V. Mamishev, IEEE Sensors Journal **6**(6), 617–620 (2006).
[7] K. Sundara-Rajan, L. Byrd, and A. V. Mamishev, IEEE Sensors Journal **4**(3), 378–383 (2004).
[8] L. Yang. M. H. Yang, and L. L. Dong, Nongye Jixie Xuebao/Transactions of the Chinese Society of Agricultural Machinery **41**(1), 77–80 (2010).
[9] T. Bore, D. Placko, F. Taillade, and P. Sabouroux, NDT & E International **60**, 110–120 (2013).
[10] Amr A. Nassr, Wael H. Ahmed, and Wael W. El-Dakhakhni, Meas. Sci. Technol. **19**, 075702 (2008).
[11] Amr A. Nassr, Wael H. Ahmed, Wael W. El-Dakhakhni, and M. Asce, Journal of Composites for Construction **13**(6), 486–497 (2009).
[12] D. Morgan, *Surface Acoustic Wave Filters-with Applications to Electronic Communications and Signal Processing* (Elsevier Ltd., 2nd edition 2007, 1st edition 1985), Chap. 5, p. 127, p. 144.
[13] H. Engan, IEEE Trans. Sonics UltrasSon. **SU-22**, 395–401 (1975).
[14] S. Datta, and B. J. Hunsinger, IEEE Trans. Sonics UltrasSon. **SU-27**, 42–44 (1980).
[15] H. Cheng, Y. Zhang, X. Huang, J. A. Rogers, and Y. Huang, Sensors and Actuators A: Physical **203**, 149–153 (2013).
[16] J. Z. Chen, A. A. Darhuber, S. M. Troian, and S. Wagner, Lab Chip. **4**(5), 473–480 (2004).
[17] T. Chen and N. Bowler, IEEE Journals & Magazines **17**(4), 1307–1318 (2010).
[18] T. Chen, N. Bowler, and J. R. Bowler, IEEE Trans. Instrum. Meas. **61**(1), 233–240 (2012).
[19] Michael E. Peskin, and Daniel V. Schroeder, *An Introduction to Quantum Field Theory* (World Publishing Corp., Beijing, 2006) Chap. 22, p. 842.